https://doi.org/10.5194/egusphere-2026-2805
Preprint. Discussion started: 2 July 2026

Conditional Modulation of Extreme Internal Solitary Waves in the Lombok Strait

Zheng Wang[1,2,3], Jiaojiao Wang[1,3], Rui Li[1,2,3], Jianing Wang[1,2,3], Weidong Ma[1,2,3], Da Wu[1,3], Adi Purwandana[4], Dwiyoga Nugroho[4], Muhammad Furqon Aziz Ismail[4], Priyadi Dwi Santoso[5], Muhammad Fadli[4], Ghelby M. Faid[1,3], Noir P. Purba[6], Umar Abdurrahman[6], Fan Wang[1,2,3]

[1] Key Laboratory of Ocean Observation and Forecasting & Laboratory of Ocean Circulation and Waves, Institute of Oceanology, Chinese Academy of Sciences, Qingdao, China

[2] Laboratory for Ocean Dynamics and Climate, Qingdao Marine Science and Technology Center, Qingdao, China

[3] University of Chinese Academy of Sciences, Beijing, China

[4] Research Center for Oceanography, National Research and Innovation Agency, Jakarta, Indonesia

[5] Research Center for Deep Sea, National Research and Innovation Agency, Jakarta, Indonesia

[6] Department of Marine Science, Faculty of Fisheries and Marine Science, Universitas Padjadjaran, Indonesia

Correspondence to: Zheng Wang (wangzheng@qdio.ac.cn)

https://doi.org/10.5194/egusphere-2026-2805
Preprint. Discussion started: 2 July 2026

Abstract.

Using 13 months of continuous mooring observations at the Lombok Strait (November 2023–December 2024), we identify 302 internal solitary wave (ISW) packets and 618 individual solitons with amplitudes up to 104 m. ISW occurrence peaks in boreal winter–spring (March: 45 packets/month) and drops to near-zero in summer (July: 3 packets/month). The observations reveal an amplitude-dependent dynamical structure. ISW occurrence for both amplitude classes is primarily modulated by the ITF: normal-amplitude ISWs (25–65 m) are seasonally suppressed during enhanced ITF periods—when thermocline stratification is concurrently elevated—indicating that the apparent negative N^2–ISW correlation is a seasonal covariance with ITF strength rather than a direct stratification effect. Extreme ISWs (>65 m) show negligible stratification dependence and instead tend to coincide with transient ITF weakening as a precondition for nonlinear amplification. Low-pass filtered acoustic Doppler current profiler records show that extreme events consistently coincide with northward velocity pulses in the 50–200 m layer that substantially reduce Doppler retardation, consistent with the existence of episodic dynamic windows favorable for nonlinear wave amplification.

https://doi.org/10.5194/egusphere-2026-2805
Preprint. Discussion started: 2 July 2026

1 Introduction

Internal solitary waves (ISWs) are large-amplitude, nonlinear disturbances that propagate along oceanic pycnoclines, transporting momentum and energy across vast distances and driving intense diapycnal mixing that influences nutrient cycling, biological productivity, and heat redistribution (Lamb, 2014; Alford et al., 2015). Although ISWs are ubiquitous in stratified marginal seas and ocean straits, the Indonesian Archipelago stands out as a global hotspot: it constitutes the only low-latitude conduit connecting the Pacific and Indian Oceans via the Indonesian Throughflow (ITF), and its complex system of narrow passages and steep sills generates some of the most energetic ISW fields on Earth (Gordon, 2005; Sprintall et al., 2009). The Lombok Strait—separating the islands of Bali and Lombok at approximately 8.5°S—is one of the three principal ITF exit passages and among the most active ISW-generation sites globally. Semidiurnal tidal currents interact with the strait's shallow sill to produce large-amplitude ISW packets that propagate predominantly northward into the Bali Sea, with isopycnal displacements of 40–100 m and phase speeds of 1.5–2.5 m s^{-1} (Susanto et al., 2005; Purwandana et al., 2021; Gong et al., 2022). These waves exert important impacts on mixing, biological productivity, acoustic propagation, and submarine navigation safety—a concern underscored by the loss of the Indonesian naval submarine KRI Nanggala-402 in these waters in 2021.

The seasonal variability of Lombok Strait ISWs has been studied almost exclusively through satellite remote sensing and numerical modeling. Mitnik et al. (2000) and

https://doi.org/10.5194/egusphere-2026-2805
Preprint. Discussion started: 2 July 2026

Susanto et al. (2005) first characterized ISW distributions using SAR imagery. Matthews et al. (2011) combined PALSAR/ERS SAR observations with numerical modeling to demonstrate that northward-propagating ISWs are far more frequent during the Northwest Monsoon (boreal winter) than the Southeast Monsoon (boreal summer), and proposed that the strong southward ITF during the Southeast Monsoon physically inhibits embryonic wave growth at the sill by constraining the northward tidal intrusion—a hydraulic-control mechanism confirmed by 2D non-hydrostatic simulations. Chonnaniyah et al. (2024) subsequently showed from multi-satellite observations that soliton numbers and phase speeds are higher during the Northwest Monsoon, consistent with shallower thermocline conditions. More recently, Zhuang et al. (2024) compiled 858 satellite images (2018–2022) and confirmed that ISW occurrence peaks in October (29% detection frequency) and is lowest in June (6%), with enhanced southward ITF corresponding to suppressed ISW occurrence and reduced northward propagation speed; three-dimensional MITgcm experiments further reproduced the suppressive effect of stronger background flow via hydraulic-control delay of ISW generation. Limited in situ data from coastal acoustic tomography (Syamsudin et al., 2019) and shipboard ADCP surveys during research cruises (Purwandana et al., 2021) have corroborated the presence of these waves, but no continuous subsurface mooring record spanning a full seasonal cycle has yet been reported.

Despite these advances, three critical gaps persist in our understanding of Lombok Strait ISW dynamics. First, all existing seasonal analyses rely on satellite remote

https://doi.org/10.5194/egusphere-2026-2805
Preprint. Discussion started: 2 July 2026

sensing, which captures only surface manifestations and cannot resolve subsurface isopycnal displacement amplitude, individual event timing, or the full water-column velocity structure. Second, the relative contributions of thermocline depth, local stratification strength (buoyancy frequency N^2), and background ITF velocity to ISW seasonal variability have never been disentangled from direct in situ observations. Third, and most critically, no study has explicitly examined whether ISWs of different amplitudes may be influenced by distinct dynamical mechanisms. Prior work implicitly treats ISW activity as controlled by a single set of environmental conditions, yet nonlinear wave theory predicts that large-amplitude waves may undergo substantial steepening and amplification through weakly nonlinear wave processes that are dynamically distinct from the linear wave generation that governs smaller events. Weakly nonlinear theory is adopted here because ISW amplitudes observed in the Lombok Strait (25–104 m, i.e., roughly 10–60% of the thermocline depth) place most events within the weakly-to-moderately nonlinear regime where amplitude-to-thermocline-depth ratios $a/h_1 \leq 0.5$, and the qualitative predictions of weakly nonlinear theory regarding the sign and direction of nonlinear steepening remain valid (Lamb, 2014). Fully nonlinear approaches (e.g., Dubreil-Jacotin–Long equation) would provide more accurate amplitude estimates for the largest events ($a/h_1 \approx 0.5$–1.0) but require complete density profiles unavailable from the present thermistor chain; this limitation is noted in the discussion (Sect. 4.4). Here we present the first analysis of ISW amplitude statistics and their amplitude-dependent seasonal dynamics from a 13-month continuous mooring observation at the Lombok Strait.

https://doi.org/10.5194/egusphere-2026-2805
Preprint. Discussion started: 2 July 2026

2 Data and Methods

2.1 Mooring Configuration

A subsurface mooring (LMK) was deployed at 8°13′31″S, 115°51′03″E in the northern Lombok Strait (water depth ~1000 m) from 20 November 2023 to 11 December 2024, providing 13 months of continuous high-frequency observations spanning a complete monsoon cycle. The mooring comprised three main components. (1) A conductivity-temperature-depth (CTD) sensor nominally at 50 m depth recorded temperature and conductivity at 1-minute intervals; the instrument was displaced to a mean depth of ~110 m by the strong downward drag of the ITF. (2) Seven thermistors at nominal depths of 70, 90, 110, 130, 150, 170, and 190 m recorded temperature at 1-minute intervals; actual depths were estimated from mooring knockdown corrections applied to pressure records. (3) An upward-looking Acoustic Doppler Current Profiler (ADCP; 75 kHz) at a nominal depth of 500 m measured three-dimensional currents in 27 bins (~16 m vertical resolution, 40–500 m range) at 2-minute intervals. All times are in Indonesian Western Time (UTC+7). Temperature and salinity observations were interpolated onto a uniform 1-minute × 1-m grid; ADCP velocity profiles were similarly gridded to 1-minute × 1-m over 40–500 m.

2.2 ISW Identification

ISWs were detected from the 18°C isotherm depth time series using an automated algorithm adapted from Gong et al. (2023). A 6-hour low-pass Butterworth filter (fourth-order) was applied to the isotherm depth to define the slowly varying

https://doi.org/10.5194/egusphere-2026-2805
Preprint. Discussion started: 2 July 2026

background thermocline state. When the 18°C isotherm was absent from the observation range for more than 6 consecutive hours, detection was switched to the 16°C isotherm (invoked for <4% of events; sensitivity tests confirm this does not alter amplitude statistics). Isotherm depth was obtained by linear interpolation between the two bracketing thermistors; time steps where the target isotherm lay outside the 70–190 m instrument range were set to missing, and gaps shorter than 6 h were bridged by linear interpolation. Mooring knockdown was corrected using pressure records from two independent sensors: the CTD pressure sensor (nominal depth 50 m, actual mean depth ~110 m due to ITF-induced displacement) and the ADCP integrated pressure sensor (nominal depth 500 m). Using two reference points is important because the depth-dependent shear of the ITF causes upper instruments to experience larger horizontal drag and hence larger knockdown than deeper instruments, so the displacement profile is non-uniform with depth. The correction procedure is:

(i) Pressure at each sensor is converted to depth via $z = p/(\rho g)$, $\rho = 1025$ kg m^{-3}, $g = 9.81$ m s^{-2}. (ii) Instantaneous knockdown displacement at each reference sensor:

$$\delta z_{\mathrm{CTD}}(t) = z_{\mathrm{CTD}}(t) - z^{\circ}_{\mathrm{CTD}}$$

$$\delta z_{\mathrm{ADCP}}(t) = z_{\mathrm{ADCP}}(t) - z^{\circ}_{\mathrm{ADCP}}$$

where z_1 (t) and z_2 (t) are pressure-derived depths at each time step and $z^{\circ}\_\mathrm{CTD} \approx 50$ m, $z^{\circ}\_\mathrm{ADCP} = 500$ m are the nominal depths.

(iii) Knockdown at each thermistor (nominal depths 70–190 m, all between the two reference sensors) is linearly interpolated:

$$\delta z_i(t) = \delta z_{\mathrm{CTD}}(t) + \frac{z^{\circ}_i - z^{\circ}_{\mathrm{CTD}}}{z^{\circ}_{\mathrm{ADCP}} - z^{\circ}_{\mathrm{CTD}}} \times [\delta z_{\mathrm{ADCP}}(t) - \delta z_{\mathrm{CTD}}(t)]$$

https://doi.org/10.5194/egusphere-2026-2805
Preprint. Discussion started: 2 July 2026

giving corrected depth:

$$z_i(t) = z_i^\circ + \delta z_i(t)$$

where $z^\circ_{CTD} \approx 50$ m and $z^\circ_{ADCP} = 500$ m are the nominal deployment depths. Linear interpolation is standard for taut wire moorings where wire stretch is negligible (Dewey, 1999).

The CTD, nominally at 50 m, experienced a sustained mean displacement of ~60 m to an actual mean depth of ~110 m due to the persistent horizontal drag of the strong ITF current; additional dynamic fluctuations of ±5–10 m around this mean occurred during tidal and ISW forcing. The ADCP at 500 m, where currents are substantially weaker, experienced dynamic displacements of 5–15 m. To separate ISW packets from large-amplitude internal tides, events were required to show an isotherm displacement rate exceeding 2.0 m min^{-1} and a peak-to-trough duration shorter than 30 min; these criteria effectively exclude the semidiurnal tidal signal (period ≈12.4 h) while retaining all identified solitary-wave events. Only depression-type events (downward isotherm displacement) were retained, consistent with the dominance of mode-1 depression waves in the Lombok Strait (Susanto et al., 2005; Matthews et al., 2011).

Two additional quality criteria were applied: (1) background isotherm stability within ±25 m of the 6-hour running mean; and (2) isotherm recovery to within 10 m of background on both flanks of the detected anomaly. Individual solitons were separated by a minimum gap of 15 min; consecutive packets required gaps of at least 90 min. All events were visually inspected via daily temperature Hovöller diagrams. The final event catalog comprises 302 wave packets and 618 individual solitons. ISW

https://doi.org/10.5194/egusphere-2026-2805
Preprint. Discussion started: 2 July 2026

amplitude was defined as the maximum isotherm depression per soliton. For packet-level statistical analyses (Sects. 3.4 and 4), each packet is represented by its peak-amplitude soliton (the largest among all solitons in the packet); the 618 individual soliton amplitudes are used for the amplitude distribution statistics only. Extreme ISWs (>65 m) correspond to the sparse high-amplitude tail of the distribution (~9% of packets), identified by a natural break in the amplitude histogram near 65 m (Supplementary Fig. S1). A sensitivity analysis shows that varying this threshold between 60 and 70 m does not qualitatively alter the conditional probability contrast or Mann–Whitney results; the 65 m value is therefore retained throughout.

2.3 Environmental Parameters and Phase Speed

Four monthly-mean environmental parameters were computed. (1) Thermocline depth: monthly-mean depths of the 18°C and 20°C isotherms by linear interpolation. (2) Local stratification: buoyancy frequency N^2 averaged within ±10 m of the 18°C isotherm, computed as $N^2 = -(g/\rho_0)(\partial\rho/\partial z)$, where ρ is computed from temperature and salinity using TEOS-10 (IOC et al., 2010) via the gsw library, with $g = 9.81$ m s^{-2} and $\rho_0 = 1025$ kg m^{-3}. (3) Background ITF velocity: monthly-mean meridional ADCP velocity averaged over 100–250 m (thermocline layer); ADCP data above 50 m were excluded due to sidelobe contamination. For time-series analysis, a 72-hour low-pass Butterworth filter isolated background flow from tidal signals. ADCP velocity records were available through 30 October 2024; for the November–December 2024 period, background meridional velocity was supplemented using daily GLORYS12 reanalysis fields (cmems_mod_glo_phy_my_0.083deg_P1D-m;

https://doi.org/10.5194/egusphere-2026-2805
Preprint. Discussion started: 2 July 2026

Copernicus Marine Service), averaged over the two model grid points nearest the mooring (115.833°E and 115.917°E, 8.333°S) and bias-corrected against the final 30-day overlap with ADCP observations. (4) Effective phase speed: estimated using a two-layer model, $c_0 = (g'h_1 h_2/(h_1 + h_2))^{1/2}$, where $g' = g(\rho_2 - \rho_1)/\rho_0$ is the reduced gravity, h_1 is the monthly-mean 18°C isotherm depth (upper layer), $h_2 = 1000 - h_1$ (lower layer, total depth H = 1000 m), and densities ρ_1, ρ_2 were computed with the TEOS-10 equation of state (IOC et al., 2010). The Doppler-corrected effective phase speed is $c^{eff} = c_0 + V_{100\text{-}250}$, where negative (southward) ITF velocity reduces c^{eff} and retards northward ISW propagation.

2.4 Statistical Analysis

Monthly ISW counts and environmental parameters were computed over 13 months (December 2023–December 2024; November 2023 excluded as partial). Pearson correlation coefficients (r) were computed between monthly ISW occurrence for two amplitude classes—normal (25–65 m) and extreme (>65 m)—and each environmental parameter, with significance assessed at $\alpha = 0.05$ (two-tailed). To quantify the background flow anomaly during extreme ISW events, the 72-hour low-pass filtered meridional velocity was averaged within ±6 hours of each extreme ISW peak time and compared against the record-mean. All analyses used Python (v3.9) with NumPy, SciPy, and Pandas. To address the small monthly sample size (n = 13), robustness of all monthly correlations was assessed using leave-one-out (LOO) analysis (n = 12 per iteration) and non-parametric bootstrap resampling (5000 iterations). Bootstrap 95%

https://doi.org/10.5194/egusphere-2026-2805
Preprint. Discussion started: 2 July 2026

confidence intervals (CIs) and permutation p-values (5000 permutations) are reported alongside parametric p-values.

3 Results

3.1 ISW Occurrence and Amplitude Statistics

Over the 13-month mooring record, 302 ISW wave packets comprising 618 individual solitons were identified. Peak amplitudes ranged from 25 to 104 m, with a mean of 40.3 m. The amplitude distribution is strongly right-skewed: small ISWs (25–45 m) account for 52.0% of all packets (n = 157), moderate ISWs (45–65 m) for 39.4% (n = 119), and extreme ISWs (>65 m) for 8.6% (n = 26). Fig. 1a–c shows the monthly distribution of each amplitude class. ISWs occurred in every month of the record, with strong seasonal modulation. The maximum occurrence was in March 2024 (45 packets/month), followed by January 2024 (39 packets/month) and August 2024 (39 packets/month). The minimum occurred in July 2024 (3 packets/month). Extreme ISWs were absent in April–July and September 2024, but reached 8 events in November 2024, suggesting that the amplitude structure of the seasonal cycle differs from that of total occurrence.

https://doi.org/10.5194/egusphere-2026-2805
Preprint. Discussion started: 2 July 2026

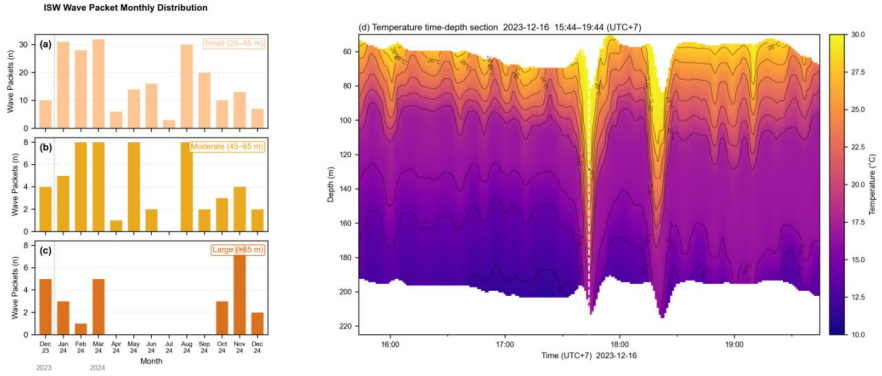

Figure 1. Monthly distribution of ISW wave packets and a representative ISW event. (a)–(c) Bar charts showing the number of ISW wave packets per month in three amplitude categories: (a) small ISWs (25–45 m; light orange), (b) moderate ISWs (45–65 m; orange), and (c) extreme ISWs (>65 m; vermillion). The dotted vertical line marks the boundary between the 2023 and 2024 portions of the record. (d) Temperature time–depth section for the representative extreme ISW event of 16 December 2023 (15:44–19:44 UTC+7), plotted using the plasma colour scale (10–30 °C). Isotherms are contoured every 2 °C. The white dashed vertical line marks the ISW peak at 17:44.

A representative extreme ISW event observed on 16 December 2023 illustrates the characteristic subsurface structure (Fig. 1d). Within a 4-hour window centered on 17:44 UTC+7, the 18°C isotherm depressed by ~80 m over the course of approximately 20 minutes, with accompanying downward displacement of the 16°C and 20°C isotherms. The temperature time–depth section reveals a classic depression ISW signature: a sharp leading front followed by a gradual return to the background

https://doi.org/10.5194/egusphere-2026-2805
Preprint. Discussion started: 2 July 2026

state, with high-frequency oscillations trailing the primary wave packet. Such events are clearly distinguishable from semidiurnal tidal oscillations in both their shorter duration (<30 min for individual solitons) and steeper isotherm displacement rates (>5 m min^{-1}).

3.2 Seasonal Variability and Environmental Parameters

Figure 2 presents the monthly co-variability of ISW occurrence, thermocline state, and internal wave energy. ISW wave packet counts (Fig. 2a) exhibit a bimodal pattern with a primary maximum in boreal winter–spring (December 2023–March 2024) and a secondary maximum in late summer (August 2024), separated by a pronounced summer minimum (July 2024: 3 packets). The extreme ISW class (>65 m, dark bars) is largely absent during April–September, even when total packet counts are moderate (e.g., August 2024: 39 total packets but only 1 extreme event).

The 18°C and 20°C isotherm depths (Fig. 2b) show a progressive deepening from December 2023 (~112 m and ~93 m, respectively) through December 2024 (~168 m and ~147 m), a net descent of ~56 m over the 13-month record. Notably, the deepest isotherm depths occur in November–December 2024 (Northwest Monsoon transition), not during the Southeast Monsoon peak (June–August 2024): the July 2024 value (~132 m) is shallower than November 2024 (~164 m), indicating that this record reflects a combination of the seasonal ITF intensification cycle and an interannual deepening trend that cannot be decomposed from a single 13-month observation. The local N^2 within ±10 m of the 18°C isotherm (Fig. 2b right axis; TEOS-10) ranges from

https://doi.org/10.5194/egusphere-2026-2805
Preprint. Discussion started: 2 July 2026

265 1.9 to 3.7 × 10^{-4} rad² s^{-2}, with a maximum in July 2024 (~3.7 × 10^{-4} rad² s^{-2}) and
266 minimum in January 2024 (~1.9 × 10^{-4} rad² s^{-2}). Notably, this window follows the
267 moving isotherm; sensitivity analysis using fixed-depth and column-maximum
268 stratification metrics yields non-significant correlations with ISW occurrence (see
269 Sect. 4.1), indicating that this N² estimate should not be interpreted as evidence of
270 direct stratification control on ISW variability.

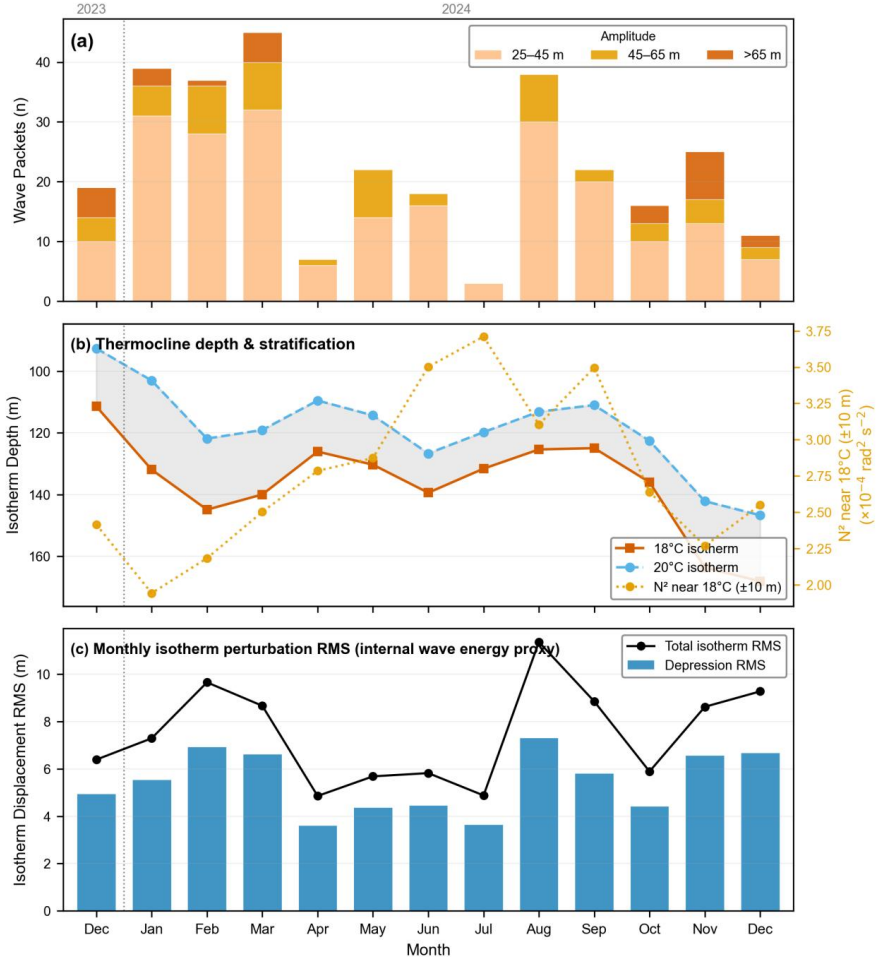

271

https://doi.org/10.5194/egusphere-2026-2805
Preprint. Discussion started: 2 July 2026

Figure 2. Seasonal variability of ISW occurrence and environmental parameters. (a) Monthly ISW wave packet counts, stacked by amplitude category: light orange = small (25–45 m), orange = moderate (45–65 m), vermillion = extreme (>65 m). (b) Monthly-mean depth of the 18 °C isotherm (vermillion squares, left axis) and 20 °C isotherm (sky-blue circles, left axis), with the grey shading indicating the thermocline layer between them. The right axis (orange dashed line with circles) shows local buoyancy frequency N^2 within ±10 m of the 18 °C isotherm, computed using TEOS-10. (c) Monthly root-mean-square (RMS) displacement of the 18 °C isotherm (blue bars: depression-type perturbations; black line: total isotherm RMS). The dotted vertical line separates 2023 and 2024.

The monthly isotherm displacement root-mean-square (RMS; Fig. 2c), used here as a proxy for total internal wave energy in the thermocline, broadly follows the ISW occurrence pattern but with important differences. The depression RMS peaks in February–March 2024 (~10 m) and again in August 2024 (~7 m), while reaching a minimum in July 2024 (~5 m). The fact that the total isotherm RMS (including both depression and elevation displacements) is consistently elevated throughout the record (5–9 m) indicates persistent internal wave activity even during the summer suppression period, consistent with continuous tidal forcing. The relatively modest suppression of total RMS in July (~5 m) compared to the near-complete absence of extreme ISWs suggests that the summer ITF does not suppress internal wave

https://doi.org/10.5194/egusphere-2026-2805
Preprint. Discussion started: 2 July 2026

generation entirely, but rather limits the nonlinear amplification required for extreme wave development.

3.3 Background Flow Compensation and Extreme ISW Events

Fig. 3 shows the 72-hour low-pass filtered meridional velocity in the upper (50–200 m) and deep (200–450 m) layers throughout the mooring record, with extreme ISW events (>65 m, black stars) and strong ISW events (58–65 m, orange circles) indicated. The upper layer (Fig. 3a) is dominated by southward (ITF) flow, with monthly-mean velocities of −0.147 m s^{-1} across the full record. However, northward velocity pulses of 0.1–0.4 m s^{-1} occur episodically, most prominently in January 2024, March 2024, and October–November 2024. These northward pulses are associated with weakening or reversal of the ITF during the transition between monsoon seasons and under the influence of intraseasonal Kelvin wave forcing from the Indian Ocean.

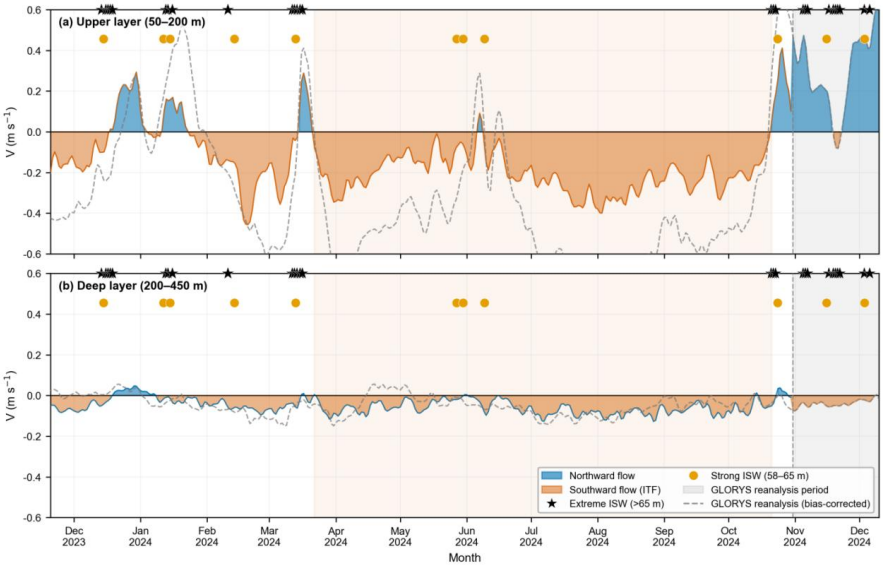

https://doi.org/10.5194/egusphere-2026-2805
Preprint. Discussion started: 2 July 2026

Figure 3. 72-hour low-pass filtered meridional velocity in the (a) upper (50–200 m) and (b) deep (200–450 m) layers throughout the mooring record. Blue shading indicates northward flow; vermillion shading indicates southward flow (Indonesian Throughflow direction). The solid line shows the ADCP-observed velocity; the grey dashed line shows bias-corrected GLORYS12 reanalysis velocity for comparison. The grey shaded region after 30 October 2024 indicates the GLORYS-extended period. Black stars mark extreme ISW events (amplitude >65 m); orange circles mark strong ISW events (58–65 m). The vermillion background shading indicates the enhanced ITF period (late March to late October 2024), determined from zero crossings of the upper-layer low-pass velocity. The grey dashed vertical line indicates the ADCP data cutoff (30 October 2024).

A clear correspondence is evident between northward velocity pulses and extreme ISW occurrence: most extreme ISW events (black stars) coincide with periods when the 50–200 m layer velocity is near-zero or weakly northward. During the enhanced ITF period (approximately April–October 2024, as determined from the zero crossings of the upper-layer low-pass velocity), the upper layer maintains persistent southward velocities of −0.2 to −0.4 m s^{-1}, and extreme ISWs are essentially absent. In contrast, the deep layer (200–450 m; Fig. 3b) shows much weaker variability (record mean: −0.051 m s^{-1}, range: −0.14 to +0.08 m s^{-1}) and no clear association with extreme ISW events, consistent with a compensation mechanism operating primarily in the thermocline layer rather than at depth.

https://doi.org/10.5194/egusphere-2026-2805
Preprint. Discussion started: 2 July 2026

Compositing the 72-hour low-pass velocity at times of extreme ISW events (±6 h around each peak) reveals a mean upper-layer velocity of +0.005 m s^{-1} during extreme events, compared to a record mean of −0.147 m s^{-1}—a difference of +0.153 m s^{-1}. The deep layer shows negligible change (+0.016 m s^{-1}). This layer-dependent pattern suggests that the Doppler retardation of northward ISW propagation, quantified as the reduction in effective phase speed $c^{eff} = c_0 + V$, may be substantially reduced during extreme events. When $V \approx 0$ m s^{-1}, the effective phase speed approaches the intrinsic linear value c_0 (1.47–2.22 m s^{-1} across our record), partially alleviating the propagation constraint and potentially opening a dynamic window for nonlinear wave growth.

3.4 Amplitude-Dependent Control Mechanisms

https://doi.org/10.5194/egusphere-2026-2805
Preprint. Discussion started: 2 July 2026

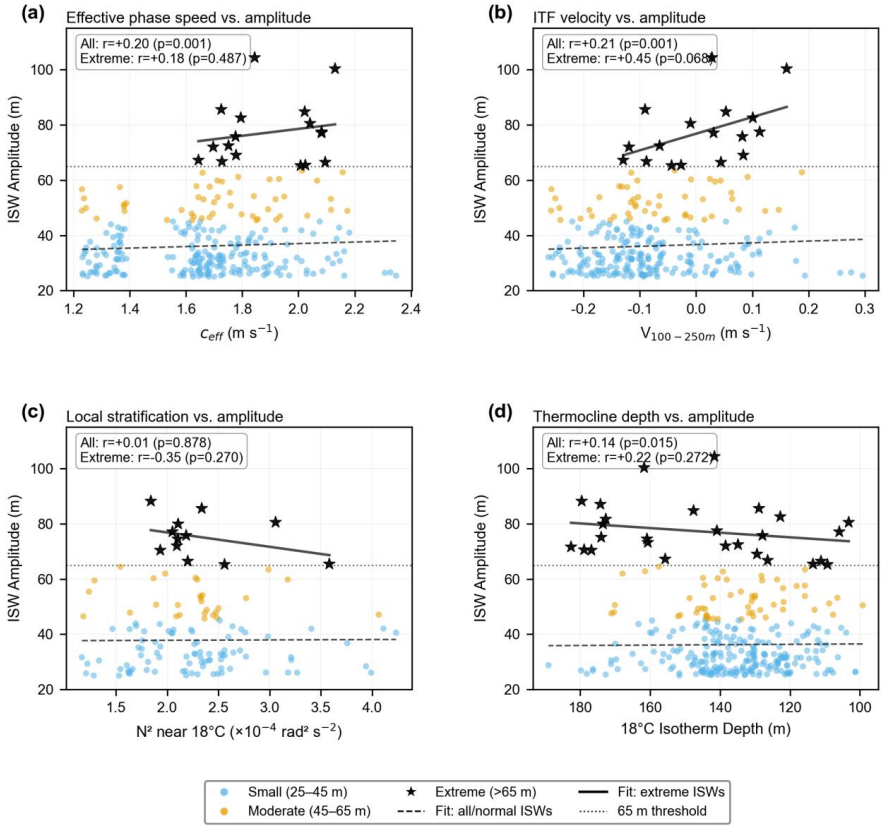

Figure 4. Event-scale relationship of ISW peak amplitude versus four environmental parameters (n = 302 wave packets, one per packet; n = 265 for panels (a)–(b) owing to the subset with concurrent ADCP records). (a) Effective phase speed c^{eff}. (b) Thermocline-layer ITF velocity $V_{100\text{-}250}$ (100–250 m; northward positive). (c) Local N^2 within ±10 m of the 18 °C isotherm. (d) Monthly-mean 18 °C isotherm depth (x-axis inverted: right = deeper thermocline). Scatter point colours indicate season: blue = December–February (Northwest Monsoon), orange = March–May, vermillion = June–August (Southeast Monsoon), purple-pink = September–November. Sky-blue circles denote small ISWs (25–45 m); orange circles denote moderate ISWs (45–65 m); black five-pointed stars denote extreme ISWs (>65 m).

https://doi.org/10.5194/egusphere-2026-2805
Preprint. Discussion started: 2 July 2026

Solid lines show statistically significant linear fits ($p < 0.05$); dashed lines show fits for the full dataset ($p \geq 0.05$). The horizontal dotted line marks the 65 m extreme ISW threshold.

Figure 4 presents event-scale scatter plots of individual ISW peak amplitude ($n = 265$ for velocity parameters, $n = 302$ for thermocline depth) against four environmental parameters measured at the time of each event: effective phase speed c^{eff} (Fig. 4a), thermocline-layer ITF velocity $V_{100\text{-}250}$ (Fig. 4b), local stratification N^2 (Fig. 4c), and 18°C isotherm depth (Fig. 4d). Stars denote extreme ISW events (>65 m). This event-scale approach avoids temporal aliasing and substantially increases statistical power. Stratification shows no significant correlation with ISW amplitude ($r = +0.01$, $p = 0.878$; Fig. 4c): extreme ISWs (stars) are distributed across the full range of observed N^2 values, indicating that thermocline strength is not the primary control on wave amplitude. In contrast, effective phase speed c^{eff} is positively correlated with amplitude ($r = +0.20$, $p < 0.001$; Fig. 4a), and extreme ISWs cluster primarily at $c^{eff} > 1.7$ m s^{-1}. ITF thermocline velocity $V_{100\text{-}250}$ is similarly significantly correlated with amplitude ($r = +0.21$, $p < 0.001$; Fig. 4b): no extreme ISW occurred when $V_{100\text{-}250} < -0.2$ m s^{-1}. Mann–Whitney U tests indicate that both c^{eff} and $V_{100\text{-}250}$ distributions differ significantly between extreme and normal ISW events ($p < 0.001$). The 18°C isotherm depth shows a weak positive correlation with amplitude ($r = +0.14$, $p = 0.015$; Fig. 4d), likely reflecting seasonal covariance between deep thermocline and weak ITF rather than a direct effect.

https://doi.org/10.5194/egusphere-2026-2805
Preprint. Discussion started: 2 July 2026

Although the Pearson correlations are modest ($r \approx 0.24$, explaining ~6% of amplitude variance), reflecting the many factors controlling ISW amplitude (tidal phase, topographic focusing, antecedent wave field), the Mann–Whitney results indicate that the background flow difference between extreme and normal ISW events is robust and statistically significant. This contrast—amplitude insensitive to stratification but responsive to ITF-induced Doppler conditions—represents an important but previously underexplored aspect of ISW dynamics in ITF-influenced passages.

4 Discussion

4.1 Re-evaluation of the N^2–ISW Relationship

The apparent negative correlation between N^2 (computed within ±10 m of the moving 18°C isotherm; Method A) and monthly ISW occurrence ($r = -0.60$, $p = 0.053$, $n = 13$ months) requires careful re-examination. This computation window moves with the isotherm as it descends from ~112 m in December 2023 to ~168 m in December 2024, meaning that N^2 estimates from different months are computed at different absolute depths. When stratification is instead measured at a fixed depth range (100–200 m; Method B), the correlation is $r = -0.51$ ($p = 0.07$) with a bootstrap 95 % CI of [−0.84, −0.09] that does not span zero (the apparent discrepancy between the CI excluding zero and the parametric $p = 0.07$ reflects small-sample uncertainty and differing assumptions: the bootstrap is non-parametric while the parametric test assumes bivariate normality at $n = 13$). Regardless of the inference approach, this

https://doi.org/10.5194/egusphere-2026-2805
Preprint. Discussion started: 2 July 2026

negative correlation is consistent with seasonal ITF co-modulation: during the Southeast Monsoon, the same ITF intensification that suppresses ISW occurrence via hydraulic control and Doppler retardation also drives thermocline deepening, elevating N^2 in the 100–200 m layer. The most direct evidence against an independent stratification effect is the event-scale scatter ($r = +0.01$, $p = 0.878$, $n = 302$): when the seasonal ITF background is removed and individual ISW events are compared, N^2 has no predictive power for ISW amplitude whatsoever. Neither the column-maximum N^2 in 50–300 m (Method C: $r = -0.10$, $p = 0.76$) nor the two-layer effective phase speed c_0 ($r = -0.39$, $p = 0.23$) shows a significant relationship with ISW occurrence, and the 18°C isotherm depth itself is essentially uncorrelated with ISW counts ($r = +0.08$, $p = 0.82$).

These results indicate that the Method A N^2–ISW correlation is an artefact of the co-movement between the tracking window and the ITF-driven thermocline. When the southward ITF intensifies, it simultaneously depresses the 18°C isotherm (shifting the ±10 m window into the thermocline core and yielding higher local N^2) and suppresses ISW occurrence via Doppler retardation and hydraulic control. The negative N^2–ISW relationship therefore reflects ITF co-modulation rather than a causal stratification effect—a conclusion consistent with the satellite-based analyses of Matthews et al. (2011) and Zhuang et al. (2024), who similarly attributed ISW suppression to ITF dynamics rather than to stratification per se. This conclusion extends to both amplitude classes: no stratification metric tested here shows a physically robust, independent correlation with ISW occurrence or amplitude. The ITF thermocline-

https://doi.org/10.5194/egusphere-2026-2805
Preprint. Discussion started: 2 July 2026

layer velocity therefore emerges as the primary physical control for both amplitude classes, operating through seasonal suppression for normal events and the episodic background flow compensation mechanism for extreme events (Section 4.2)..

4.2 Background Flow Compensation Mechanism for Extreme ISWs

The decoupling of ISW amplitude from stratification ($r = +0.01$, $p = 0.878$), and its conditional clustering relationship with ITF velocity ($r = +0.21$, $p < 0.001$, $n = 265$ events), suggests the presence of a distinct physical mechanism operating for the largest wave events. We propose that this reflects a background flow compensation process in which episodic reductions of the southward ITF—driven by intraseasonal Kelvin waves propagating from the Indian Ocean (Matthews et al., 2011; Arief & Murray, 1996) or by the seasonal ITF weakening during the Northwest Monsoon transition—temporarily reduce the Doppler retardation that normally constrains northward ISW propagation speed. When the thermocline-layer velocity approaches zero ($c^{eff} \approx c0$), the nonlinear steepening timescale, which scales as $(\alpha A)^{-1}$ in weakly nonlinear theory where α is the nonlinearity parameter and A is wave amplitude, becomes short relative to the propagation timescale over the strait width. Under such conditions, initial tidal disturbances or baroclinic tidal beams may steepen into large-amplitude solitons.

The quantitative observational evidence for this mechanism is broadly consistent with the proposed mechanism. During extreme ISW events, the upper-layer background velocity is $+0.005$ m s^{-1} (effectively zero), compared to the record mean of

https://doi.org/10.5194/egusphere-2026-2805
Preprint. Discussion started: 2 July 2026

−0.147 m s⁻¹. The corresponding increase in effective phase speed $\Delta c^{eff} \approx +0.15$ m s⁻¹ is dynamically meaningful: given a typical intrinsic phase speed of $c_0 \approx 1.7$–2.2 m s⁻¹ in our record, the mean ITF-induced retardation of 0.15 m s⁻¹ represents a 7–10% reduction in effective propagation speed. While modest in absolute terms, this retardation is sufficient to alter the phase relationship between the generating tidal forcing and the nascent wave disturbance, potentially modulating the efficiency of energy extraction at the sill—consistent with the hydraulic-control timing mechanism described by Zhuang et al. (2024). Furthermore, the absence of a significant deep-layer (200–450 m) velocity anomaly during extreme events (+0.016 m s⁻¹) indicates that the compensation is confined to the thermocline layer, precisely where the ISW orbital velocities and mode-1 baroclinic shear are strongest. Note that the monthly-mean thermocline-layer velocity shows no significant correlation with monthly ISW packet counts ($r = -0.06$, $p = 0.86$; LOO range [−0.28, +0.09]), confirming that the ITF control operates at the event scale rather than through a simple monthly-mean relationship. The amplitude-based event-scale analysis ($n = 265$; Sect. 3.4) therefore provides the more direct and relevant test of the proposed mechanism.

4.3 Implications for ISW Hazard Assessment

The background flow compensation mechanism has practical implications for ISW hazard prediction. Previous satellite-based approaches have relied on monsoon phase or stratification indices as proxies (Zhuang et al., 2024; Chonnaniyah et al., 2024), which are adequate for normal-amplitude ISWs but insufficient for anticipating extreme events. Real-time monitoring of thermocline-layer ITF velocity—from

https://doi.org/10.5194/egusphere-2026-2805
Preprint. Discussion started: 2 July 2026

satellite altimetry or moored ADCPs—may potentially provide a more direct indicator of elevated extreme ISW risk, though the limited record length (13 months) precludes formal validation of predictive skill, particularly during the October–November transition period when ITF weakening and extreme ISW occurrence most frequently coincide (Gong et al., 2022).

4.4 Limitations and Future Work

Several limitations of the present study warrant acknowledgement. First, our 13-month record, while sufficient to capture a full seasonal cycle, precludes assessment of interannual variability. ITF transport is known to vary significantly with ENSO and the Indian Ocean Dipole (Matthews et al., 2011; Hu et al., 2022), and these interannual signals are expected to modulate both the mean ITF strength and the frequency of intraseasonal velocity pulses. Multi-year mooring records would be required to assess whether the amplitude-dependent mechanisms identified here are robust across ENSO phases. Second, with only a single mooring, we cannot directly observe the ISW generation process at the sill or track individual wave packets from generation to the observation point. The inferred hydraulic-control mechanism remains physically plausible based on the velocity anomaly composites, but direct verification would require an array of moorings spanning the sill and the northern strait. Third, the two-layer model used to estimate effective phase speed is a simplification; in reality, the vertical mode structure of ISWs in the Lombok Strait is influenced by the continuously stratified water column and the depth-varying ITF shear profile. More sophisticated estimates using continuously stratified weakly

https://doi.org/10.5194/egusphere-2026-2805
Preprint. Discussion started: 2 July 2026

nonlinear theory (e.g., Yang et al., 2021) could better quantify the nonlinear amplification potential under varying background conditions. To assess robustness, we extended the event-scale dataset to include 37 additional ISW events from November–December 2024 using GLORYS12-supplemented background velocity ($n = 337$ total; 10 additional extreme events). The correlations with $V_{100\text{-}250}$ ($r = +0.22$, $p < 0.001$) and c^{eff} ($r = +0.26$, $p < 0.001$) remain highly significant, indicating that the background flow compensation mechanism is not sensitive to the choice of data source for the extended observation period.

5 Conclusions

We have presented the first continuous subsurface mooring analysis of internal solitary wave (ISW) seasonal variability and amplitude-dependent dynamics in the Lombok Strait, based on 13 months of concurrent thermistor and ADCP observations (November 2023–December 2024). The key conclusions are as follows.

1. ISW occurrence is strongly seasonal, peaking in boreal winter–spring (March 2024: 45 wave packets/month) and reaching a minimum in boreal summer (July 2024: 3 packets/month). Over the full record, 302 wave packets and 618 individual solitons were identified, with amplitudes ranging from 25 to 104 m.

2. A sensitivity analysis of stratification metrics reveals that the apparent N^2–ISW correlation from the moving-window estimate ($r = -0.60$, $p = 0.05$) is a methodological artefact: when N^2 is computed at a fixed depth (100–200 m) or as the column maximum (50–300 m), correlations with ISW occurrence are non-significant

https://doi.org/10.5194/egusphere-2026-2805
Preprint. Discussion started: 2 July 2026

(r = −0.43 and −0.10 respectively, both p > 0.1); the 18°C isotherm depth itself is also uncorrelated with ISW counts (r = +0.08, p = 0.82). Stratification is therefore not an independent control factor for ISW occurrence in either amplitude class. The moving-window N^2 co-varies with ISW occurrence because the ITF simultaneously depresses the isotherm (raising local N^2) and suppresses ISW generation via Doppler retardation, producing a spurious correlation.

3. Extreme ISWs (>65 m, ~9% of all packets) appear dynamically decoupled from stratification (r = −0.25, p = 0.417) and instead showed a tendency to coincide with weakened ITF thermocline-layer velocity (monthly-scale r = +0.57, p = 0.066; marginal). The event-scale scatter plot (Fig. 4b) yields r=+0.45 (p=0.07) for extreme-class ISWs only, measuring amplitude modulation by concurrent ITF velocity—a distinct analysis from the monthly-scale correlation cited above. Seventy-two-hour low-pass filtered ADCP records show that extreme events tend to coincide with near-zero or northward velocity pulses in the 50–200 m layer (composite mean: +0.005 m s^{-1} versus record mean of −0.147 m s^{-1}), while the deep layer (200–450 m) shows negligible change.

4. We propose a background flow compensation mechanism in which episodic weakening ITF is hypothesized to reduce Doppler retardation of northward ISW propagation, potentially creating dynamic windows for nonlinear wave amplification. The proposed mechanism appears to be amplitude-selective: it appears to govern the generation of extreme events while leaving the production of normal-amplitude ISWs — which is primarily suppressed by seasonal ITF intensification rather than by

https://doi.org/10.5194/egusphere-2026-2805
Preprint. Discussion started: 2 July 2026

episodic ITF weakening — largely unaffected by the compensation mechanism. This duality—seasonal ITF suppression for normal ISWs, episodic ITF compensation for extreme ISWs—represents an important but previously underexplored aspect of ISW dynamics in ITF-influenced passages and has implications for ISW hazard assessment and seasonal prediction in the Lombok Strait .

Financial support. This study is supported by the Strategic Priority Research Program of the Chinese Academy of Sciences (XDB42000000), the MFA Construction and Demonstration of Sino-Indonesian Ecological Marine Ranching Program, the CAS-ANSO Sustainable Development Research Project (CAS-ANSO-SDRP-2024-02), and the National Natural Science Foundation of China (41906012).

Author contributions. ZW conceived and designed the study, led the mooring deployment and recovery, performed the data analysis, and wrote the manuscript. JJW and GMF contributed to data processing and visualization. RL, WDM, DW, NPP, and UA contributed to fieldwork and data collection. AP, DN, MFI, PDS, and MF led the Indonesian research coordination and cruise operations. JNW and FW provided scientific guidance and reviewed the manuscript. All authors reviewed and approved the final manuscript.

Acknowledgements

We express our gratitude to the captain and crew on RV Geomarin III for their outstanding performance and invaluable support throughout the cruises. We also want

https://doi.org/10.5194/egusphere-2026-2805
Preprint. Discussion started: 2 July 2026

to thank the IMPOLSE joint cruise between IOCAS and BRIN. This collaboration work is facilitated by the platform of Sino-Indonesia Joint Laboratory for Marine Sciences (SIMS). A.P. thanks the President's International Fellowship Initiative (PIFI) Program of the Chinese Academy of Sciences; D.N. thanks the ANSO visiting fellowship program. Artificial intelligence tools (Claude) were used to assist with language editing and text refinement. The authors are fully responsible for the scientific content and interpretations presented.

Code and data availability

The mooring data (CTD, temperature and ADCP) and derived ISW detection results used in this study can be requested at http://dx.doi.org/10.12157/IOCAS.20260428.001. The GLORYS12 reanalysis data (dataset: cmems_mod_glo_phy_my_0.083deg_P1D-m) used to extend the background velocity time series for November – December 2024 are freely available from the Copernicus Marine Service: https://data.marine.copernicus.eu/product/GLOBAL_MULTIYEAR_PHY_001_030/description, DOI: https://doi.org/10.48670/moi-00021

Competing interests

The authors declare that they have no conflict of interest.

References

https://doi.org/10.5194/egusphere-2026-2805
Preprint. Discussion started: 2 July 2026

Alford, M. H., Peacock, T., MacKinnon, J. A., Nash, J. D., Buijsman, M. C., Centurioni, L. R., and coauthors: The formation and fate of internal waves in the South China Sea, Nature, 521, 65–69, https://doi.org/10.1038/nature14399, 2015.

Chonnaniyah, Osawa, T., As-Syakur, A. R., Karang, I. W. G. A., and da Silva, J. C.: On the distinction of seasonal internal solitary waves characteristics in the Lombok Strait based on multi-satellite data, Int. J. Remote Sens., 45, 8742–8757, https://doi.org/10.1080/01431161.2023.2242592, 2024.

Dewey, R.: Mooring Design & Dynamics—a Matlab® package for designing and analyzing oceanographic moorings, Marin. Sci., 1, 103-157, https://doi.org/10.1016/S1369-9350(00)00002-X, 1999.

Gong, Q., Chen, L., Diao, Y., Xiong, X., Sun, J., and Lv, X.: On the identification of internal solitary waves from moored observations in the northern South China Sea, Sci. Rep., 13, 3133, https://doi.org/10.1038/s41598-023-28565-5, 2023.

Gong, Y., Xie, J., Xu, J., Chen, Z., He, Y., and Cai, S.: Oceanic internal solitary waves at the Indonesian submarine wreckage site, Acta Oceanologica Sin., 41, 109–113, https://doi.org/10.1007/s13131-021-1893-0, 2022.

Gordon, A. L.: Oceanography of the Indonesian seas and their throughflow, Oceanography, 18, 14–27, https://doi.org/10.5670/oceanog.2005.01, 2005.

IOC, SCOR, and IAPSO: The international thermodynamic equation of seawater – 2010: Calculation and use of thermodynamic properties, Intergovernmental

https://doi.org/10.5194/egusphere-2026-2805
Preprint. Discussion started: 2 July 2026

Oceanographic Commission, Manuals and Guides No. 56, UNESCO, 196 pp., 2010.

Lamb, K. G.: Internal wave breaking and dissipation mechanisms on the continental slope/shelf, Annu. Rev. Fluid Mech., 46, 191–223, https://doi.org/10.1146/annurev-fluid-011212-140701, 2014.

Matthews, J. P., Aiki, H., Masuda, S., Awaji, T., and Ishikawa, Y.: Monsoon regulation of Lombok Strait internal waves, J. Geophys. Res. Oceans, 116, C05007, https://doi.org/10.1029/2010JC006403, 2011.

Mitnik, L., Alpers, W., and Lim, H.: Thermal plumes and internal solitary waves generated in the Lombok Strait studied by ERS SAR, in: ERS-Envisat Symposium: Looking Down to Earth in the New Millennium, pp. 16–20, European Space Agency, 2000.

Purwandana, A., Cuypers, Y., and Bouruet-Aubertot, P.: Observation of internal tides, nonlinear internal waves and mixing in the Lombok Strait, Indonesia, Cont. Shelf Res., 216, 104358, https://doi.org/10.1016/j.csr.2021.104358, 2021.

Sprintall, J., Wijffels, S. E., Molcard, R., and Jaya, I.: Direct estimates of the Indonesian Throughflow entering the Indian Ocean: 2004–2006, J. Geophys. Res. Oceans, 114, C07001, https://doi.org/10.1029/2008JC005257, 2009.

Susanto, R. D., Mitnik, L., and Zheng, Q.: Ocean internal waves observed in the Lombok Strait, Oceanography, 18, 80–87, https://doi.org/10.5670/oceanog.2005.08, 2005.

https://doi.org/10.5194/egusphere-2026-2805
Preprint. Discussion started: 2 July 2026

610 Syamsudin, F., Taniguchi, N., Zhang, C., Hanifa, A. D., Li, G., Chen, M., and
611 coauthors: Observing internal solitary waves in the Lombok Strait by coastal
612 acoustic tomography, Geophys. Res. Lett., 46, 10475–10483,
613 https://doi.org/10.1029/2019GL084595, 2019.
614 Yang, Y., Huang, X., Zhao, W., Zhou, C., Huang, S., Zhang, Z., and Tian, J.: Internal
615 solitary waves in the Andaman Sea revealed by long-term mooring
616 observations, J. Phys. Oceanogr., 51, 3609–3627, https://doi.org/10.1175/JPO-
617 D-20-0310.1, 2021.
618 Zhuang, C., Li, X., Shen, D., and Zhang, X.: Internal solitary wave in the Lombok
619 Strait: Satellite-observed spatiotemporal characteristics and their propagations
620 modulated by the Indonesian Throughflow, Ocean Model., 190, 102398,
621 https://doi.org/10.1016/j.ocemod.2024.102398, 2024.